Supporting Online Material for

Tunability and Noise Dependence in Differentiation Dynamics

Gürol M. Süel, Rajan P. Kulkarni, Jonathan Dworkin,
Jordi Garcia-Ojalvo, Michael B. Elowitz*

*To whom correspondence should be addressed. E-mail: melowitz@caltech.edu

Published 23 March 2007, *Science* **315**, 1716 (2007)
DOI: 10.1126/science.1137455

This PDF file includes:

Supporting Online Text

Tunability and noise dependence in differentiation dynamics

Gürol M. Süel[1], Rajan P. Kulkarni[2], Jonathan Dworkin[3], Jordi Garcia-Ojalvo[4] and Michael B. Elowitz[2]

[1]*Green Center Division for Systems Biology and Department of Pharmacology, University of Texas Southwestern Medical Center*

[2]*Division of Biology and Department of Applied Physics, California Institute of Technology, Pasadena, CA 91125*

[3]*Department of Microbiology, College of Physicians and Surgeons, Columbia University New York, NY 10032*

[4]*Departament de Física i Enginyeria Nuclear, Universitat Politècnica de Catalunya, Colom 11, E-08222 Terrassa, Spain*

S1. Modeling of the competence circuit

S1.1. **Continuous model**

The core competence circuit depicted in Fig. 1B involves two interacting proteins, the competence master regulator ComK and the small peptide ComS, coupled through competitive degradation by the protease MecA. The dynamics of this circuit can be represented, in a continuous description, in terms of the following two coupled differential equations for the concentrations K and S of ComK and ComS, respectively:

$$\begin{aligned}\frac{dK}{dt} &= \alpha_k + \frac{\beta_k K^n}{k_k^n + K^n} - \frac{\delta_k K}{1 + K/\Gamma_k + S/\Gamma_s} - \lambda_k K \\ \frac{dS}{dt} &= \alpha_s + \frac{\beta_s}{1 + (K/k_s)^p} - \frac{\delta_s S}{1 + K/\Gamma_k + S/\Gamma_s} - \lambda_s S\end{aligned} \qquad \text{(S1)}$$

In the ComK equation, the first term in the right-hand side represents constitutive expression of the P_{comK} promoter, measured by α_k. This promoter has a non-zero basal activity in wild-type cells, which is augmented in a controlled way in the Hyper-α_k strain described in the main text. The second term on the right-hand side represents the positive transcriptional autoregulation by

ComK of its own gene. In the ComS equation, the constant α_s term describes the effect of the additional constitutive P_{comS} promoter in the Hyper-α_s strain, while the second term describes inhibition of *comS* expression by ComK. The overall strength of the P_{comS} promoter, measured by β_s, is related to the stress level, since competence-inducing conditions trigger the activation of ComA, whose phosphorylated form activates in turn ComS expression [1].

In both the ComK and ComS equations, the third term corresponds to competitive binding to MecA, and the last term represents linear degradation, with coefficients λ_k and λ_s, respectively. The strength of competitive binding is measured by the parameters δ_k and δ_s for ComK and ComS, respectively. The affinity of the two proteins for MecA is given by the EC_{50} values Γ_k and Γ_s, respectively.

The model is obtained upon adiabatic elimination of the dynamics of MecA and its complexes with ComK and ComS [2], and can be recast in dimensionless form by rescaling the dependent and independent variables:

$$K' = \frac{K}{\Gamma_k}, \qquad S' = \frac{S}{\Gamma_s}, \qquad t' = \delta_k t \qquad \text{(S2)}$$

Assuming $\delta_k = \delta_s$ and dropping the primes for simplicity, we obtain:

$$\begin{aligned} \frac{dK}{dt} &= a_k + \frac{b_k K^n}{k_0^n + K^n} - \frac{K}{1+K+S} - \Delta_k K \\ \frac{dS}{dt} &= a_s + \frac{b_s}{1+(K/k_1)^p} - \frac{S}{1+K+S} - \Delta_s S \end{aligned} \qquad \text{(S3)}$$

Here, the following dimensionless parameters have been defined:

$$\begin{aligned} a_k &= \frac{\alpha_k}{\Gamma_k \delta_k}, \quad b_k = \frac{\beta_k}{\Gamma_k \delta_k}, \quad k_0 = \frac{k_k}{\Gamma_k}, \quad \Delta_k = \frac{\lambda_k}{\delta_k} \\ a_s &= \frac{\alpha_s}{\Gamma_s \delta_s}, \quad b_s = \frac{\beta_s}{\Gamma_s \delta_s}, \quad k_1 = \frac{k_s}{\Gamma_k}, \quad \Delta_s = \frac{\lambda_s}{\delta_s} \end{aligned} \qquad \text{(S4)}$$

S1.2. **Constraining parameter space with experimental observations**

The dynamical behavior of model (S3) can be determined by a phase-plane analysis. Figure S1 shows the location of the nullclines $\frac{dK}{dt} = 0$ and $\frac{dS}{dt} = 0$ in the *K*-*S* plane, together with the slope field as determined from the right-hand side of the equations (S3). For the parameters given in Table S1, the nullclines cross at three points, the left-most of which is stable and corresponds to the vegetative fixed point. The other two fixed points are unstable (the middle one is a saddle, and the right-most one is an unstable spiral fixed point). The structure of the slope field is such that relatively small horizontal perturbations of the vegetative state (notice the logarithmic character of the *x*-axis in Fig. S1) cause the system to undergo large excursions in phase space (see grey trajectories in the right panel of the figure). This is the hallmark of excitability. These trajectories correspond to competence events, where ComK levels increase transiently. Excitability in Fig. S1 requires the existence of these three fixed points.

The particular phase-plane scenario exhibited by this system is equivalent, for instance, to type I excitable behavior in neurons [3]. This type of excitability is characterized by being born with a vanishing firing frequency. The phenomenon was originally observed by A. Hodgkin in 1948 [4], and has been studied since then both by neurophysiologists [5] and by applied mathematicians [6].

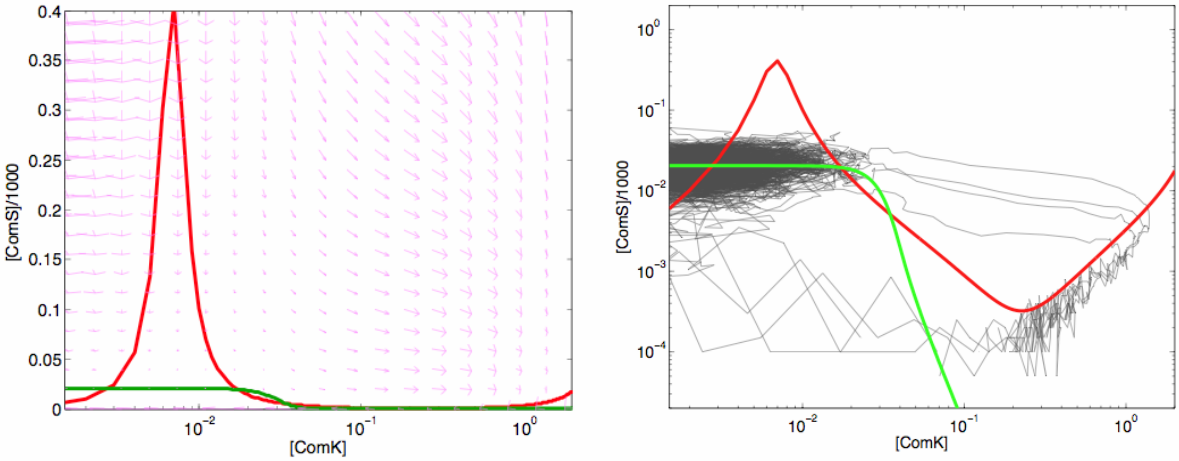

Figure S1: **Phase-plane analysis of the competence circuit.** The red line represents the nullcline of ComK and the green line the nullcline of ComS. Both semilogarithmic (left) and log-log (right) plots are shown. Magenta arrows in the left plot show the slope field, while the thin gray lines in the right plot are sample trajectories generated by the discrete model described below. The axis represent *dimensionless* concentrations of ComK and ComS, as defined in Eq. (S2).

Experimental observations, described in the main text, have shown a remarkable resilience of the competence phenotype for a wide range of strengths of the P_{comS} promoter. The 6xS strain has an approximately six-fold increase in ComS expression (β_S) compared to wild-type cells (see section S2.3 below), yet still exhibits excitable competence events. This observation places a strong constraint on the model. The ComS nullcline (green line in Fig. S1) shifts vertically upwards as the strength of the P_{comS} promoter (β_S) increases. At very high β_S, the two left-most fixed points collide and disappear, eliminating excitability. The large peak in the ComK nullcline (red line in Fig. S1) permits the ComS nullcline to shift over a large vertical range, as *comS* expression is varied, and still maintain the three fixed points. Thus, it allows the model to maintain excitability for the experimentally observed range of β_S values.

This requirement constrains the values of model parameters. We performed a systematic exploration of parameter space, searching for parameter sets that simultaneously exhibit excitability and are robust to six-fold changes in β_S with respect to wild-type values. We found that these dynamical constraints are much stronger than standard steady-state constraints, and led to a set of dimensionless parameters around the values given in Table S1.

a_k	0.00035	k_0	0.2
a_s	0.0	k_1	1/30
b_k	0.3	Δ_k	0.1
b_s	3.0	Δ_s	0.1

Table S1: **Dimensionless parameters of the continuous model.**

In spite of the strength of the dynamical constraints mentioned above, the size of the parameter region is not small, in relative terms. Figure S2 shows the effect on P_{init} and τ_{comp} of 20% changes in the values of the most sensitive parameters in Table S1 (see main text and section S.1.4 for the precise definition of these quantities). As shown in the figure, excitability is maintained in the whole parameter range, and the variation in these two quantifiers are not substantial. The influence of other parameters (specifically a_k, a_s and b_s) on these two properties is described below (section S.1.4).

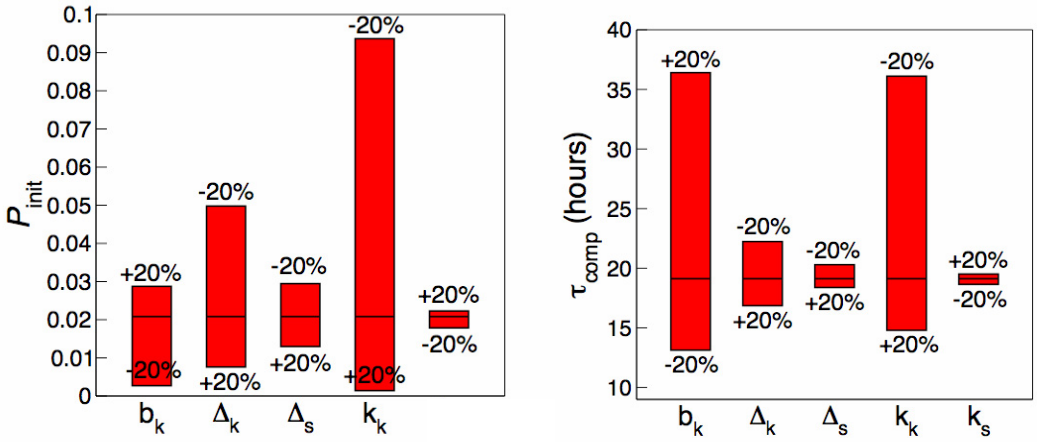

Figure S2: **Sensitivity of the excitable regime to parameter variations.** The effect of increasing or decreasing by 20% the values of indicated parameters of the dimensionless model (Eq. S3) on P_{init} (left) and τ_{comp} (right).

Besides excitability, the model described above allows other types of dynamical behaviors. Figure S3 shows a phase diagram of this model in the a_k-a_s plane. Regions of monostable, bistable and oscillatory behavior exist. Although the wild-type system represented by this model exhibits excitability (competent events), other dynamical behaviors can also be observed, as shown experimentally in the main text. The different regions are bounded by well defined transitions. For instance, the line between the vegetative (V/E) and the oscillatory (O) regions corresponds to a saddle-node on invariant circle (SNIC) bifurcation [3], while the transition between the latter and the competent (C) regime is given by a Hopf bifurcation. The following transitions occur via saddle-node bifurcations: (B1 and C/E), (V/E and B2), (B2 and B3), (B3 and C/E), and (C/E and C). Finally, the transition between C/E and O is also mediated by a saddle-node on invariant circle (SNIC) bifurcation [3].

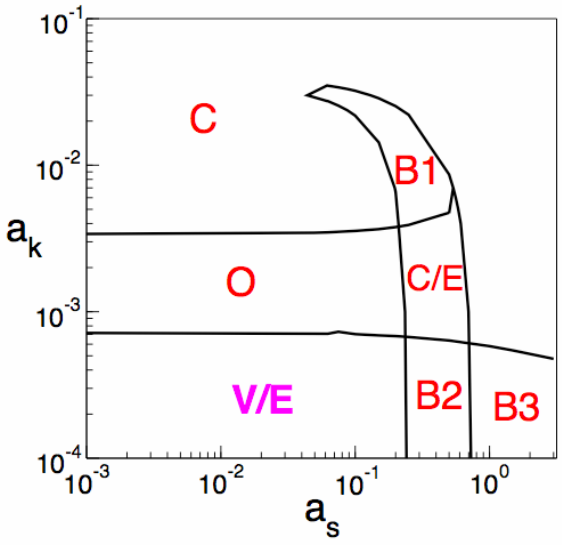

Figure S3: **Phase diagram of the continuous competence model.** Different dynamical regimes in the a_k-a_s plane are denoted as follows: V/E, vegetative/excitable regime; O, oscillatory regime; C, stable competence regime; B1, coexistence of two stable competent states, with different (but both relatively high) levels of ComK; C/E, "inverse" excitable regime, where the rest state is competent (i.e. with high ComK levels); B2 and B3, coexistence of vegetative and competence states, the difference between them being the number of unstable states. All lines were computed with the continuation software AUTO (http://indy.cs.concordia.ca/auto/).

Phase-plane plots portraying the model nullclines and sample trajectories are shown in Fig. S4, for all regions appearing in the phase diagram of Fig. S2. These phase portraits also show the different types of fixed points exhibited by each regime, and the stable and unstable manifolds of the saddle points.

S1.3. **Discrete stochastic model**

As shown in the main text, competence events are driven by noise. In order to explicitly take intrinsic noise sources into account, we developed a stochastic model of the core competence circuit depicted in Fig. 1B. The relationship between the stochastic and continuous models is described below. Our model does not include sources of noise extrinsic to the circuit, and reproduces the main features of the experimental system. In what follows we describe the set of reactions that underlie the competence circuit.

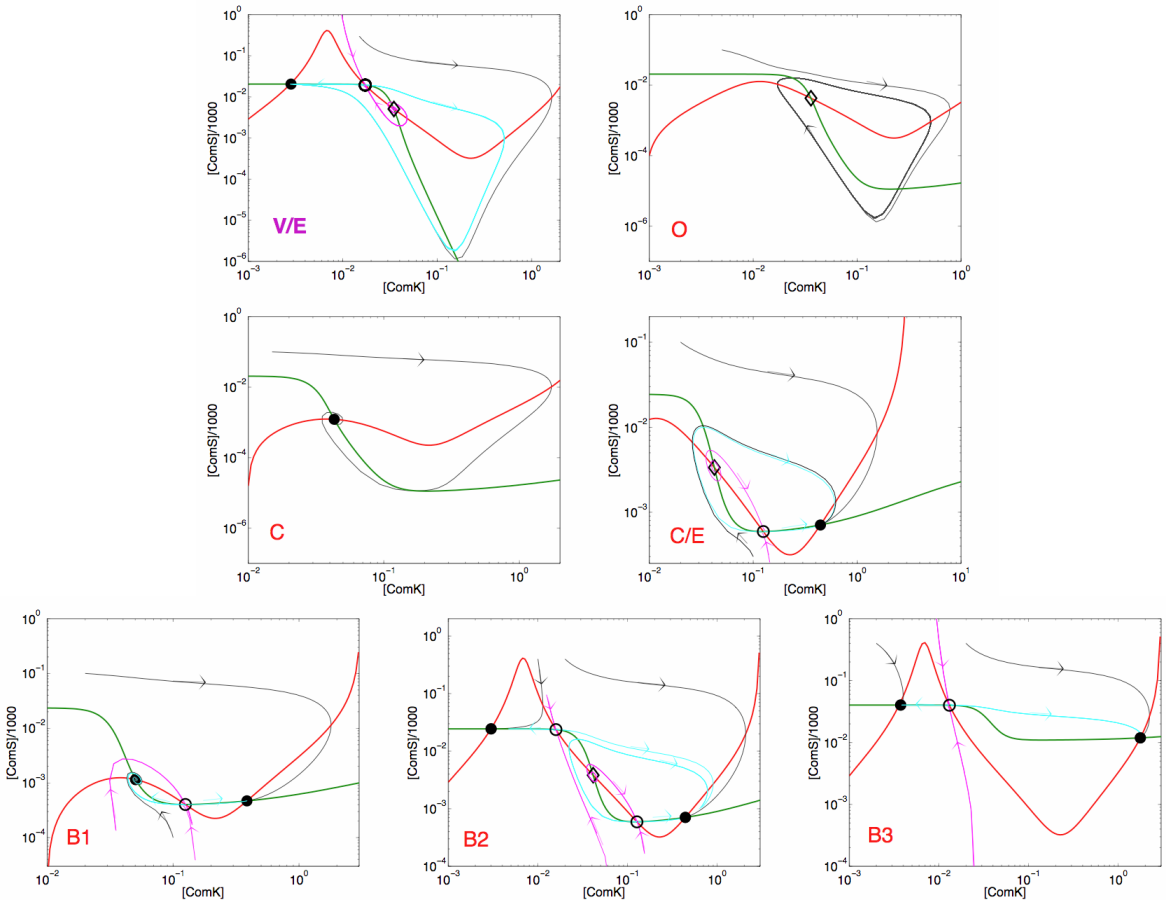

Figure S4: **Phase plane plots of dynamical regimes exhibited by the model.** Red (green) lines denote ComK (ComS) nullclines, and black lines represent sample trajectories. Stable fixed points are denoted by full circles, saddle points by empty circles, and other unstable fixed points (both nodes and foci) by empty diamonds. The unstable (stable) manifolds of the saddle points are represented by cyan (magenta) lines. The different regimes are labeled as in Fig. S3. Parameters are those of Table SI, except: **O**, a_k=0.001, a_s=0.01; **C/E**, a_k=0.001, a_s=0.4; **B1**, a_k=0.01, a_s=0.3; **B2**, a_k=0.00035, a_s=0.4; **B3**, a_k=0.00035, a_s=2.

Expression of *comK* is governed by the following reactions:

$$\begin{aligned} \mathrm{P}_{comK}^{\mathrm{const}} &\xrightarrow{k_1} \mathrm{P}_{comK}^{\mathrm{const}} + \mathrm{mRNA}_{comK} \\ \mathrm{P}_{comK} &\xrightarrow{f(K,k_2,k_k,n)} \mathrm{P}_{comK} + \mathrm{mRNA}_{comK} \\ \mathrm{mRNA}_{comK} &\xrightarrow{k_3} \mathrm{mRNA}_{comK} + \mathrm{ComK} \end{aligned} \qquad \text{(S5)}$$

where $\mathrm{P}_{comK}^{\mathrm{const}}$ and P_{comK} represent the constitutive and regulated promoters of the *comK* gene, respectively. Similarly, the expression of ComS is described by:

$$\begin{aligned} \mathrm{P}_{comS}^{\mathrm{const}} &\xrightarrow{k_4} \mathrm{P}_{comS}^{\mathrm{const}} + \mathrm{mRNA}_{comS} \\ \mathrm{P}_{comS} &\xrightarrow{g(K,k_5,k_s,p)} \mathrm{P}_{comS} + \mathrm{mRNA}_{comS} \\ \mathrm{mRNA}_{comS} &\xrightarrow{k_6} \mathrm{mRNA}_{comS} + \mathrm{ComS} \end{aligned} \qquad \text{(S6)}$$

The rates of regulated transcription of ComK and ComS are assumed to be given by the following Hill functions:

$$f(K,k_2,k_k,n)=\frac{k_2K^n}{k_k^n+K^n},\qquad g(K,k_5,k_s,p)=\frac{k_5}{1+(K/k_s)^p}\qquad \text{(S7)}$$

Here k_k (k_s) is the activation (repression) coefficient defined in Eq. (S1), and represents the concentration of ComK for which its own activation (repression) is half-maximal. While the discrete model is written in terms of molecule numbers, the Hill functions (S7) involve the *concentrations* of ComK and ComS. The relation between concentrations and molecule numbers is given by the following factor:

$$\Omega = V A = 1.66\,\mu\text{m}^3 \times 6.023\cdot 10^{23}\,\text{molec/mol} = 1\ \text{molec/nM}$$

where A is Avogadro's number, and V is the cell volume, which we assume here to have a value of 1.66 μm^3.

The use of the Hill functions defined in Eq. (S7) constitutes an approximation to the transcription dynamics of ComK and ComS, which substantially speeds up the simulations, and reduces the number of parameters in the model. We have checked that explicitly describing the cooperative DNA binding/unbinding (microscopic) reactions underlying these transcription processes does not change the results reported in this paper.

The two mRNA and protein species are also assumed to be subject to linear degradation:

$$\begin{aligned} &\text{mRNA}_{comK} \xrightarrow{k_7} \varnothing \qquad && \text{ComK} \xrightarrow{k_8} \varnothing \\ &\text{mRNA}_{comS} \xrightarrow{k_9} \varnothing \qquad && \text{ComS} \xrightarrow{k_{10}} \varnothing \end{aligned} \qquad \text{(S8)}$$

Finally, the two proteins bind to MecA competitively, and become degraded by the protease:

$$\begin{aligned} &\text{MecA} + \text{ComK} \xrightarrow{k_{11}/\Omega} \text{MecA\_K} \qquad && \text{MecA} + \text{ComS} \xrightarrow{k_{13}/\Omega} \text{MecA\_S} \\ &\text{MecA} + \text{ComK} \xleftarrow{k_{-11}} \text{MecA\_K} \qquad && \text{MecA} + \text{ComS} \xleftarrow{k_{-13}} \text{MecA\_S} \\ &\text{MecA\_K} \xrightarrow{k_{12}} \text{MecA} \qquad && \text{MecA\_S} \xrightarrow{k_{14}} \text{MecA} \end{aligned} \qquad \text{(S9)}$$

Note that the rates of the bimolecular reactions are divided by the volume factor Ω defined above. This is necessary because the stochastic description is made in terms of molecule numbers, while the differential equation description refers to protein concentrations [7].

In order to relate the reaction rates of the stochastic model with the parameters of the corresponding continuous model, described in Sec. S1.1, one can write down the differential equations associated with the different reactions, taking into account the conversion from molecule numbers to concentrations. Finally, adiabatic eliminations are performed to reduce the problem to two coupled differential equations, which when compared with Eqs. (S1) yield the following identities. For the expression parameters:

$$\alpha_k = \frac{k_1 k_3}{k_7}\left[\mathrm{P}_{comK}^{\mathrm{const}}\right] = \frac{k_1 k_3}{k_7}\frac{\mathrm{P}_{comK}^{\mathrm{const}}}{\Omega}, \qquad \beta_k = \frac{k_2 k_3}{k_7}\left[\mathrm{P}_{comK}\right] = \frac{k_2 k_3}{k_7}\frac{\mathrm{P}_{comK}}{\Omega}$$
$$\alpha_s = \frac{k_4 k_6}{k_9}\left[\mathrm{P}_{comS}^{\mathrm{const}}\right] = \frac{k_4 k_6}{k_9}\frac{\mathrm{P}_{comS}^{\mathrm{const}}}{\Omega}, \qquad \beta_s = \frac{k_5 k_6}{k_9}\left[\mathrm{P}_{comS}\right] = \frac{k_5 k_6}{k_9}\frac{\mathrm{P}_{comS}}{\Omega} \qquad \text{(S10)}$$

Here, square brackets denote concentrations, and the promoter copy numbers, denoted P^{x}_{y}, are made explicit. Similarly, the parameters quantifying the competitive degradation process obey the following relations:

$$\Gamma_k = \frac{k_{-11} + k_{12}}{k_{11}} \qquad \delta_k = k_{12}\left[\mathrm{M_T}\right]\frac{k_{11}}{k_{-11} + k_{12}}$$
$$\Gamma_s = \frac{k_{-13} + k_{14}}{k_{13}} \qquad \delta_s = k_{14}\left[\mathrm{M_T}\right]\frac{k_{13}}{k_{-13} + k_{14}} \qquad \text{(S11)}$$

Here $[\mathrm{M_T}]$ represents the total concentration of MecA molecules, assumed constant. Finally, the linear degradation parameters are unchanged with respect to the continuous model:

$$\lambda_k = k_8, \qquad \lambda_s = k_{10} \qquad \text{(S12)}$$

Starting from the dimensionless parameters of Table S1, for which a phase-plane analysis of the continuous model indicates the existence of excitability, and using the scaling relations given in Eqs. (S4), one can establish reasonable values for the real-unit parameters appearing in model (S1). Next, one can use relations (S10)-(S12) together with reasonable assumptions for some of the parameters (such as the mRNA and protein lifetimes) to reach a set of microscopic parameters that are consistent with an excitable phenotype. An example of such a set of parameters is given in Table S2. Trajectories generated by this parameter set using Gillespie's stochastic simulation algorithm [7] are shown superimposed on the right panel of Fig. S1.

k_1	0.00021875 s^{-1}	k_7	0.005 s^{-1}	k_{12}	0.05 s^{-1}
k_2	0.1875 s^{-1}	k_8	10^{-4} s^{-1}	k_{13}	$4.5\cdot10^{-6}$ $nM^{-1}s^{-1}$
k_3	0.2 s^{-1}	k_9	0.005 s^{-1}	k_{-13}	$5\cdot10^{-5}$ s^{-1}
k_4	0	k_{10}	10^{-4} s^{-1}	k_{14}	$4\cdot10^{-5}$ s^{-1}
k_5	0.0015 s^{-1}	k_{11}	$2.02\cdot10^{-6}$ $nM^{-1}s^{-1}$	k_k	5000 nM
k_6	0.2 s^{-1}	k_{-11}	$5\cdot10^{-4}$ s^{-1}	k_s	833 nM

Table S2: **Parameters of the discrete stochastic model.**

S1.4. **Model predictions I: perturbing parameter values**

We performed sets of simulations for varying values of some of the parameters, in conjunction with experiments described in the main text. In these simulations we analyzed the statistics of competence events by means of two observables:

1. The *probability of initiation* of competence, P_{init}, defined as the probability per cell cycle that a cell becomes competent. In the simulations, we estimated P_{init} in the following way: For a fixed number of realizations leading to one competent event each, we calculated the time needed for initiation to occur. Assuming a cell-cycle time of 4 hours,

we translated the activation time into the corresponding number of cell divisions that have occurred until competence arises. Dividing the total number of competent events observed (equal to the total number of realizations) by the total number of cell divisions required we obtain a measure of P_{init} comparable to those observed experimentally.

2. The competence duration, τ_{comp}, calculated as the time during which the number of ComK molecules exceeds a certain amount, 10^4 in our case. The results shown below do not vary qualitatively when this arbitrary threshold is chosen to have a different value.
3. The probability of reinitiation, defined as the probability that a cell, after coming out of the competent state, goes back into it after a fixed amount of time, in our case taken to be equal to two cell cycles. A value of this quantity close to 1 indicates the oscillatory character of the dynamics.
4. The probability of exit, defined as the fraction of competent cells that eventually leave the competent state. This observable allows us to determine whether a cell is stuck in competence.

In each simulation realization, the system was left to equilibrate during a "warm-up" time of around 140 hours, starting from arbitrary initial conditions. In order to avoid having a competence event occurring right at the end of the warm-up time, and thus starting the observation time with the cell being competent already, we artificially augmented the volume of the system 10-fold during the warm-up period, which reduced the noise (see below) and prevented any competent initiation in that period.

Experimentally, three parameters were varied in a controlled way: In the Hyper-α_k strain, addition of varying amounts of IPTG allowed us to control the basal expression of *comK*. This corresponds to parameter α_k in the continuous model (S1), or to the rate k_1 in (S5). Systematic variation of this parameter allowed us to determine within the model, the effect of the basal expression of *comK* on the statistics of competence. The results are shown, together with the corresponding experimental observations, in Fig. 2E of the main text, and in more detail in Fig. S5. Increasing basal expression of *comK* increases the probability of competence initiation up to 100%, without significantly affecting the duration of competence. This is similar to the experimental results shown in Fig. 2.

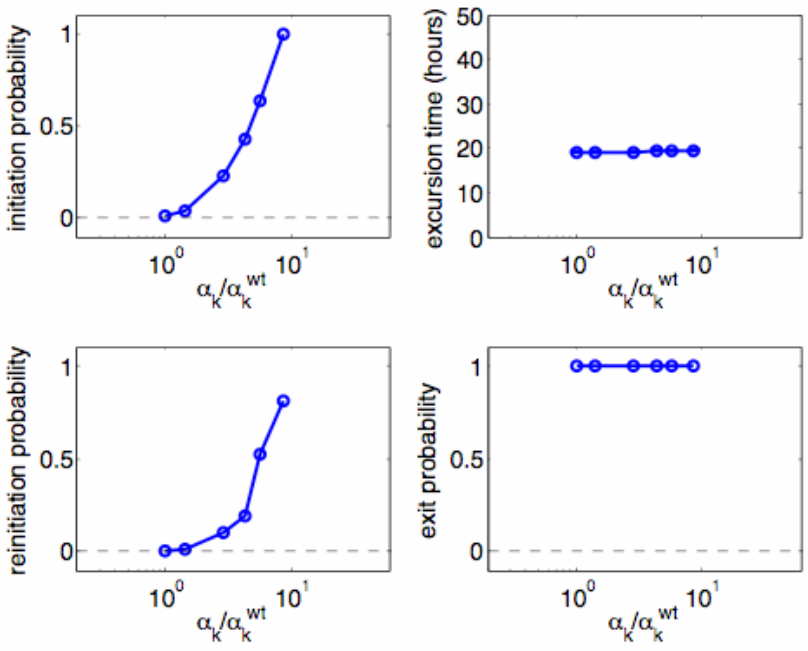

Figure S5: **Effect of ComK expression on the statistics of competence.** Constitutive expression of *comK*, α_k, is systematically increased, and measured in units of its wild-type level. The four panels show the effects of this increase on P_{init}, τ_{comp}, probability of reinitiation, and probability of exit.

Figure S5 also shows that for increasing α_k the increase in probability of initiation is associated with an increase in the probability of reinitiation, and thus with more frequent oscillations. Furthermore, the probability of exit is 1 for all values of α_k that lead to either excitability or oscillations. For larger α_k values, not shown in the figure, the cells are stuck in competence.

A second set of experiments involved the Hyper-α_S strain, where an inducible promoter controls the expression of the P_{comS} promoter. Such a perturbation corresponds in the model to increasing α_s (Eq. S1), or analogously the reaction rate k_4 (Eq. S6). As shown in Fig. S6, increasing α_s does not affect the probability of initiation, but does increase τ_{comp}. The probability of re-initiation is zero in the whole range of α_s, which means that no oscillatory behavior is observed, in contrast to effects of α_k shown in Fig. S5. No oscillatory regime is observed at intermediate α_s, in agreement with experimental observations.

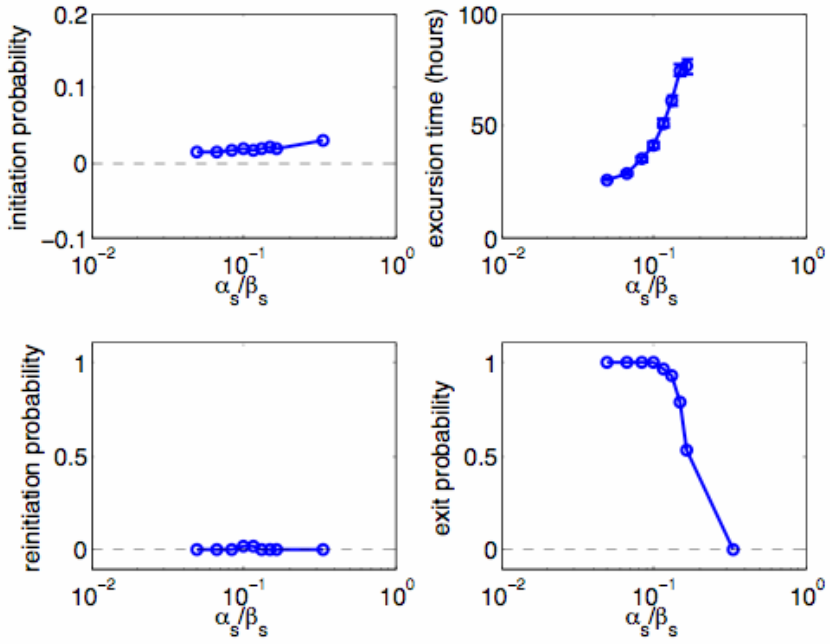

Figure S6: **Effect of ComS expression on the statistics of competence.** The four panels show the effects of α_s on the probability of initiation, competence duration, probability of reinitiation and of exit. α_s is measured in units of β_s

Control of competence duration. The effect of α_s on competence duration can be understood by comparing the trajectories in phase space of the wild-type and high-α_s cases (Fig. S7). The trajectories were generated by the discrete model, and are superimposed on the nullclines of the corresponding continuous model. The numbers of ComK and ComS molecules are transformed into dimensionless concentrations via Eq. (S2). The plots are double logarithmic, and the scaling is such that in the lower part of the trajectories, the discreteness of the molecule numbers is apparent. In the wild-type case, competence excursions take the system through regions of phase space where no attractors are present, but at high α_s, the ComS nullcline (green line) shifts upwards and ends up crossing the ComK nullcline (red line) in a region of high ComK, creating two new fixed points. Of these two new fixed points, the one at the left is unstable, while the right-most one is stable, and the system can reside in it temporarily until stochastic fluctuations induce the system to escape from this (metastable) competent state. This behavior produces an extended plateau in ComK levels which delays exit from competence. Such a plateau is similar to experimental observations (Fig. 2 in the main text).

The transition between the two extreme situations depicted in Fig. S7 is represented in the right plot of Fig. S8. That plot shows that, even before the new competent fixed point is created, the ComS nullcline bends upwards and creates a bottleneck in phase space, between the two nullclines and in the region around the future location of the two new fixed points. That bottleneck produces a substantial increase in the duration of the competence excursions. The probability of initiation, on the other hand, is determined by the separation between the vegetative fixed point at low ComK levels, and the unstable saddle on its right. The right plot of Fig. S8 shows that the distance between these two fixed points is basically unchanged with a_s, and therefore the probability of initiation does not vary either. The opposite picture arises for increasing a_k, shown in the left plot of Fig. S8: the probability of initiation is strongly affected by

that parameter, while the structure of phase space at high ComK levels, which determines the duration of competence, doesn't change much.

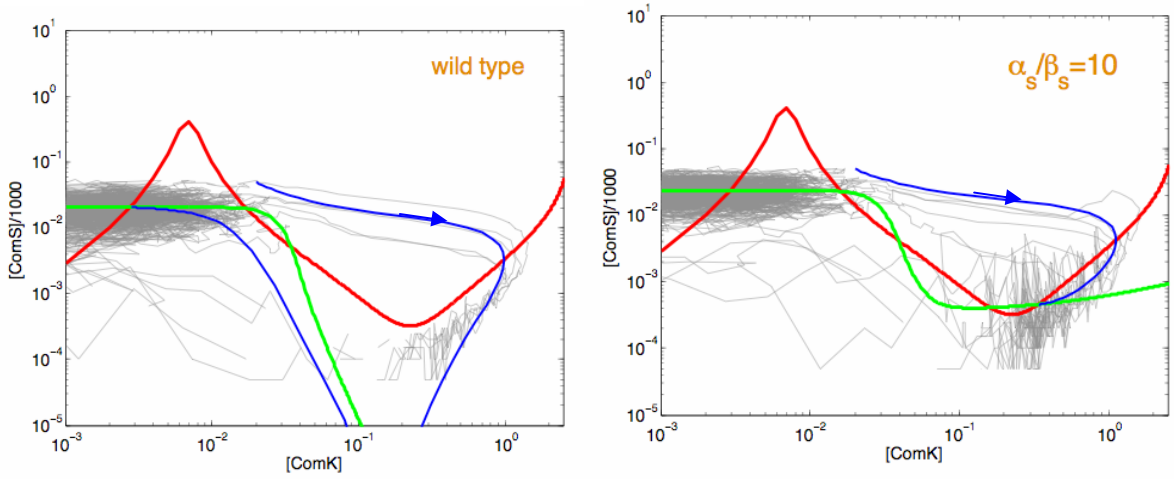

Figure S7: **Phase-plane trajectories during competence events.** Trajectories generated by discrete simulations, shown in grey, are superimposed to the ComK and ComS nullclines (red and green, respectively), for both wild type and a high constitutive expression of *comS*. Deterministic trajectories are shown in blue. In the higher α_s case, the deterministic trajectory gets trapped in the competence fixed point (intersection of blue, green, and red lines).

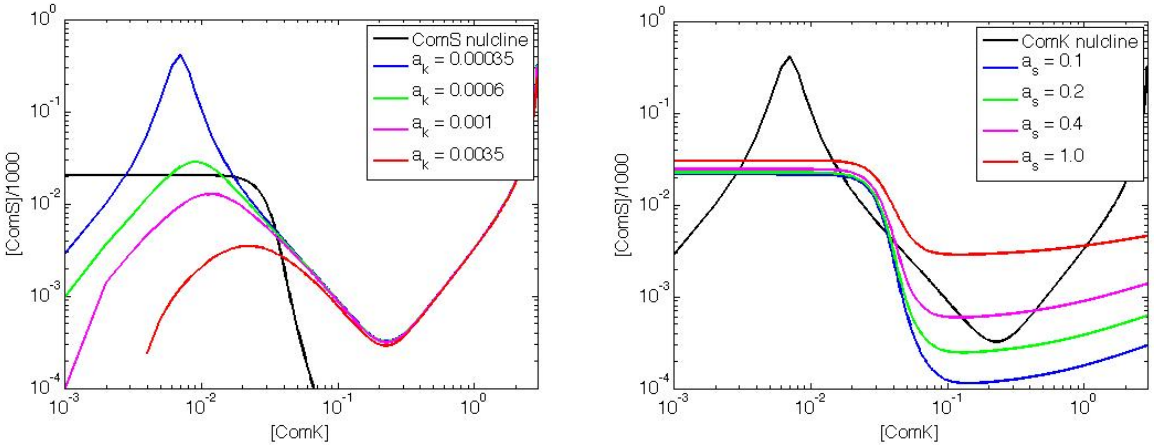

Figure S8: **Nullcline variation for increasing strength of the basal transcription of ComK and ComS.** Variation in the nullclines of the dimensionless model (Eq. S3) with increasing basal expression of ComK (left) and ComS (right). The fixed nullcline (ComS in the left plot and ComK in the right plot) is represented in black; the varying nullclines are color coded as shown in the legends.

Effects of β_S. The 6xS strain was used to determine the effect of an ~6-fold increase in the strength of the regulated P_{comS} promoter (β_s) on competence (see main text). Within the model, β_s has an effect intermediate between those of α_k and α_s. Increasing β_s causes τ_{comp} to increase much more rapidly than the probability of initiation, as is the case with α_s. However, the increase in β_s also promotes oscillation, as measured from the probability of reinitiation, an effect similar to that induced by increasing α_k (see Fig. S9).

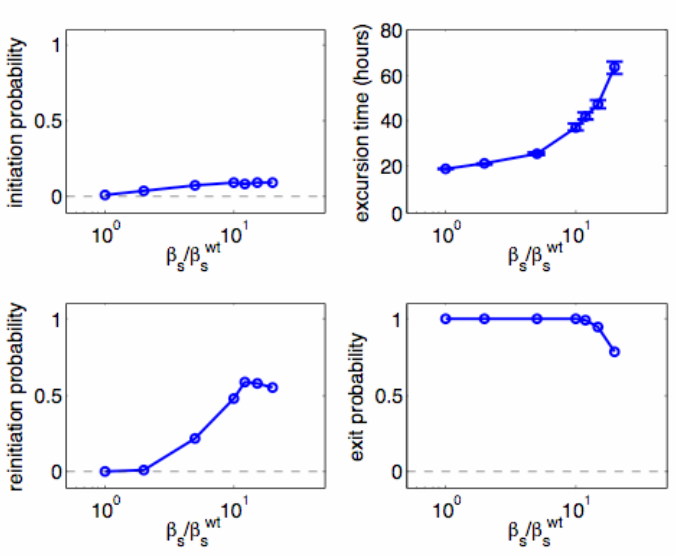

Figure S9: **Effect of regulated ComS expression on the statistics of competence.** β_s, measured in units of its wild-type value, was systematically increased. The four panels show the effects of this increase on P_{init}, τ_{comp}, the probability of reinitiation and the probability of exit.

S1.5. **Model predictions II: perturbing circuit architecture**

The CompRok strain was used experimentally to study the effect of perturbing the architecture of the circuit. In this strain, a well-known repressor of ComK, *rok*, was placed under the control of the P_{comG} promoter, which is thought to be activated exclusively by ComK [8]. In order to describe this new interaction, we introduced two new species in our discrete model, namely the mRNA and protein of the *rok* gene, and their corresponding transcription, translation and degradation reactions:

$$\begin{aligned} &\mathrm{P}_{rok} \xrightarrow{f(K,k_2,k_k,n)} \mathrm{P}_{rok} + \mathrm{mRNA}_{rok} \\ &\mathrm{mRNA}_{rok} \xrightarrow{k_3} \mathrm{mRNA}_{rok} + \mathrm{Rok} \\ &\mathrm{mRNA}_{rok} \xrightarrow{k_7} \varnothing \\ &\mathrm{Rok} \xrightarrow{k_8} \varnothing \end{aligned} \qquad \text{(S13)}$$

Here we have assumed that the reaction rates involved with the generation and degradation of Rok are equal to the corresponding ones for ComK. Finally, taking into account the inhibitory effect that Rok has on *comK* expression, the transcription reaction of the latter (second reaction in Eq. S5) is rewritten as:

$$\mathrm{P}_{comK} \xrightarrow{h(K,R,k_2,k_k,k_{15},k_r,n)} \mathrm{P}_{comK} + \mathrm{mRNA}_{comK} \qquad \text{(S14)}$$

where h is the following combinatorial Hill function:

$$h(K,R,k_2,k_k,k_{15},k_r,n) = \frac{1}{1+(R/k_r)^n}\frac{k_{15}K^n}{k_k^n + K^n} \qquad \text{(S15)}$$

In the simulations shown in the paper (Fig. 3), we used k_{15}=0.1875 s^{-1} and k_r=20 μM. The model shows that adding this extra link to the competence circuitry decreases the mean duration of competence events and reduces its variability (Fig. 3 in the main text). In order to understand the mechanism through which these effects arise, we compare in Fig. S10 the temporal evolution of ComK and ComS for multiple competence events, for both the wild-type and CompRok strains. The figure shows that, in wild-type, ComS needs to completely disappear before the cell can exit competence. In the CompRok strain, on the other hand, direct transcriptional inhibition of ComK eliminates that requirement, i.e. ComS need not be degraded completely before exiting competence. This fact has two main consequences: (i) the competent events are shorter (on average) in the CompRok strain than in the wild-type, and (ii) in the wild-type case, the duration is more susceptible to fluctuations because it relies on reducing ComS levels to very low absolute numbers, where stochastic fluctuations become significant. This does not happen in the CompRok strain, where ComS levels are never very low.

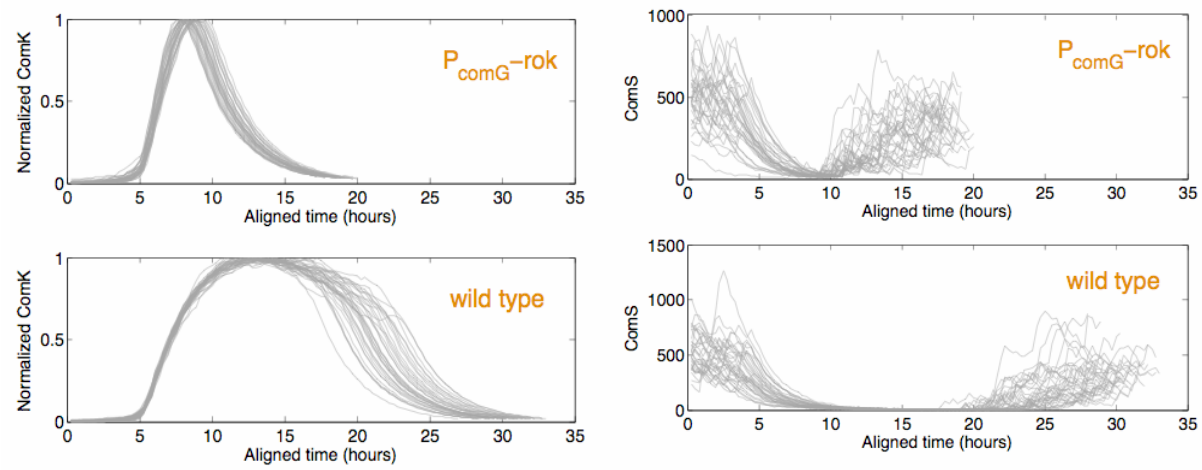

Figure S10: **Adding a negative feedback loop to ComK via Rok.** Multiple time traces of ComK (left panels) and ComS (right panels) for both the wild-type (bottom) and CompRok (top) strains. ComK has been normalized to the maximum of each time trace to ease comparison.

S1.6. **Model predictions III: controlling noise**

In order to show that increasing the cell volume reduces noise, we developed a simple model of transcription and translation in a growing cell. The cell is assumed to grow (and hence replicate its DNA) but not divide, similar to the phenotype of the conditional *ftsW* mutant strain analyzed in this paper.

The model involves constitutive transcription of mRNA, at a rate proportional to the number N_{chrom} of chromosomes of the cell, and translation of the mRNA at a rate proportional to both N_{chrom} and to the concentration of mRNA. Finally, the mRNA decays with a half-life on the order of minutes, while the protein is stable, its concentration decaying only by dilution:

$$\begin{aligned} \mathrm{P}_X &\xrightarrow{k_1} \mathrm{P}_X + \mathrm{mRNA}_X \\ \mathrm{mRNA}_X &\xrightarrow{k_2} \mathrm{mRNA}_X + \mathrm{X} \\ \mathrm{mRNA}_X &\xrightarrow{k_3} \varnothing \end{aligned} \qquad \text{(S16)}$$

In order to take into account the increase in the number or chromosomes, the rate k_1 of the transcription reaction is considered to be proportional to N_{chrom}, while the rate of translation is proportional to N_{chrom}/V, with V being the cell volume. Under these conditions, the variability in the concentration of protein, X/V, can be measured (Fig. 4 of the main text). The parameters used in those simulations were, in arbitrary units, k_1=1.5, k_2=50, k_3=10. Additionally, the volume and number of chromosomes were assumed to grow geometrically, duplicating every cell cycle time (equal to 5 arbitrary units).

Once the decrease in noise with increasing volume was demonstrated, by means of experimental observation in filamentous cells together with simulations of the previous model, we proceeded to study the effect of cell growth on competence. Using the model described in Sec. S1.3, we varied the volume of the cell, as determined by the parameter Ω. Such a volume change affects the rates of bimolecular reactions (see Eqs. S9). Furthermore, all expression rates (α_k, α_s, β_k, and β_s) are proportional to the chromosome number N_{chrom} and all translation rates are considered proportional to both N_{chrom} and the density of the corresponding mRNA species. We verified that mean concentrations were not affected by this transformation. Under these conditions, the model shows that P_{init} decreases with cell volume (Fig. 4D). This decrease becomes faster, as shown in Fig. S11, when the model assumes that the chromosome number grows continuously instead of geometrically. The restriction to discrete values for chromosome number causes an additional source of cell-cycle driven variability, as described elsewhere [9].

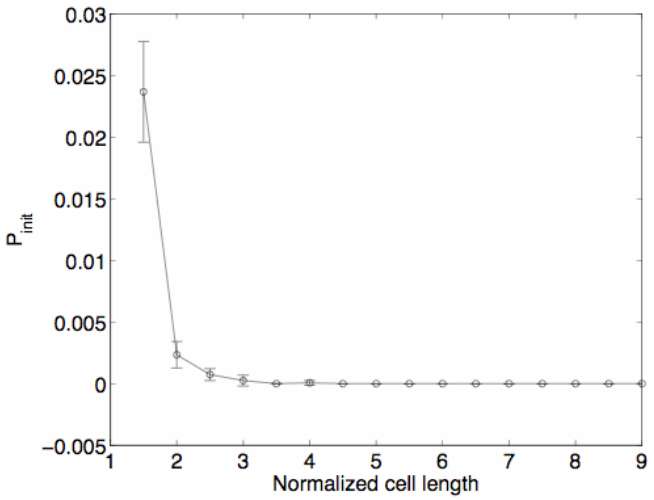

Figure S11: **Effect of continuous and non-integer DNA replication on the dependence of initiation probability on cell length.** Here we make the non-physical assumption that chromosome number increases continuously in time (and can have fractional values), in contrast with the geometric increase considered in the rest of this section, and accounting for synchronous replication of DNA along the filamenting cell. This figure should be compared with Fig. 4D of the main text.

S2. Materials and methods

S2.1. **Strain construction**

All strains listed below were derived from the wild type *Bacillus subtilis* PY79 strain. Indicated constructs were integrated chromosomally into *B. subtilis* using the following standard integration vectors and respective chromosome integration sites: Vector ECE174, which integrates into the *sacA* site (constructed by R. Middleton and obtained from the *Bacillus* Genetic Stock Center), vector ECE173, which integrates into the *gltA* site (constructed by R. Middleton and obtained from the *Bacillus* Genetic Stock Center) and vector pDL30, which integrates into the *amyE* site.

Table S3. **List of strains:**

Name:	**Genotype:**	**Shown in figure:**
Hyper-αK	*amyE*:: P_{hyp}-*comK* *sacA*::P_{comG}-*cfp*-P_{comS}-*yfp*	Fig. 2A
Hyper-αS	*amyE*:: P_{hyp}-*comS* *sacA*::P_{comG}-*cfp*-P_{comS}-*yfp*	Fig. 2B
6xS	*amyE*::P_{comG}-cfp-P_{comS}-*yfp* pHP13::P_{comS}-*comS*	
pHP13-reporter	pHP13::P_{comG}-*cfp*-P_{comS}-*yfp*	
CompRok	*amyE*::P_{comG}-cfp-P_{comS}-*yfp* *sacA*:: P_{comG}-*rok*	Fig. 3B
Fili-H (P_{hyp}-*yfp*)	*thrC*::P_{xyl}- *ftsW* mls *ftsW*::tet *sacA*::P_{hyp}-*yfp*	
Fili-SOG (P_{spo0A}-*mcherry*/ P_{comG}-*cfp*/ P_{comS}-*yfp*)	*amyE*:: P_{spank}-*ftsW* spec *ftsW*::tet *sacA*:: P_{comG}-*cfp*-P_{comS}-*yfp* *gltA*::P_{spo0A}-*mcherry*	Fig. 4C

S2.2. **Promoter definitions**

All native *B. subtilis* promoters were amplified from the chromosomal regions listed below using Polymerase Chain Reaction (PCR). P_{hyp} and P_{xyl} refer to IPTG and Xylose inducible promoters respectively (kind gifts of David Rudner (Harvard Medical School).

- P_{comG}: chromosomal sequence 2559328 to 2559937 (complementary orientation)
- P_{comS}: chromosomal sequence 375645 to 376505 (direct orientation)
- P_{spo0A}: chromosomal sequence 2518061 to 2518502 (direct orientation)

First, to each promoter the Ribosome Binding Site (RBS) sequence AAGGAGGAA was added (incorporated into PCR primers). Second, the promoter was fused to either the indicated fluorescent protein coding sequence, or alternatively *comK*, *comS* or *rok* coding sequences as indicated.

S2.3. **Construction of the conditional *ftsW* strain**.

To construct the xylose-inducible conditional *ftsW* strain, the *ftsW* gene and RBS were cloned into a *thrC* derivative of plasmid pOR277 [10] and integrated into the chromosome by double cross-over integration at *thrC*. The endogenous *ftsW* gene was then deleted (*ftsW*::*tet*) by constructing a plasmid containing sequences 5' and 3' of the *ftsW* gene flanking a tet^R cassette. This plasmid was then transformed into *B. subtilis* carrying the *thrC*::P_{xyl}-*ftsW*, and selecting for tet^R in the presence of 0.5% xylose. The integration was tested by genetic linkage and PCR to confirm that it occurred at *ftsW*. To construct the IPTG dependent *ftsW* strain, the *ftsW* gene and RBS were cloned into the *amyE* integration pSpank plasmid (pDR111) and the plasmid was integrated into the *B. subtilis* chromosome, selecting for $spec^R$. DNA from the strain containing the *ftsW*::*tet* was then transformed into the P_{spank}-*ftsW* strain, selecting for tet^R in the presence of 1mM IPTG.

S2.4. ***Bacillus* pHP13 plasmid and 6xS strain**

The pHP13 low copy number *Bacillus* plasmid was a kind gift of Beth A. Lazazzera (UCLA). To determine the copy number of pHP13 in single cells, we first inserted our P_{comG}-*cfp*-P_{comS}-*yfp* construct into the multiple-cloning-site of pHP13 using EcoRI and BamHI restriction sites. We then transformed PY79 with this plasmid and obtained the pHP13-reporter strain. Quantification of P_{comG}-*cfp* and P_{comS}-*yfp* fluorescence levels in the pHP13-reporter strain were compared to chromosomally integrated P_{comG}-*cfp* and P_{comS}-*yfp* fluorescence levels. This calibration indicated a copy number of ~5 copies of pHP13 per *B. subtilis* cell (data not shown).

The 6xS strain was constructed as follows: We integrated the P_{comS} -*comS* construct into the multiple-cloning-site of pHP13 using EcoRI and BamHI restriction sites and obtained the pHP13::P_{comS} –*comS* plasmid. We then transformed the PY79 strain which contained the chromosomally integrated P_{comG}-*cfp* and P_{comS}-*yfp* reporters with the pHP13- P_{comS} –*comS* plasmid and obtained the 6xS strain (for genotype see Table S3 above).

S2.5. **Description of the filamentous *Fili* strain**

The conditional *ftsW* mutation in Fili-H and Fili-SOG strains prevents segmentation and results in elongation of cells during growth. In Fili-SOG and Fili-H strains the *ftsW* phenotype can be rescued by inducing expression of additional FtsW from an IPTG or Xylose inducible promoter respectively (for genotype information of Fili strains see Table S3 above). Removal of the respective inducer (IPTG or Xylose) induces filamentous growth. Fili-H and Fili-SOG strains of cell lengths greater than 20 were prone to lysis with increasing cell length.

S2.6. **Distribution of chromosomal DNA in Fili strains**

To verify the assumption that in Fili strains the number of chromosomes scales with cell length and that chromosomal DNA is distributed regularly, we used DAPI staining. Fili cells that contain no fluorescent reporters were pre-lengthened to various cell lengths and then stained for 5 minutes with 1mM DAPI and washed twice with PBS following standard protocol. As can be seen in Figure S12 below, the number of chromosomes in Fili strains scales with length. Furthermore, the distribution of chromosomal DNA in Fili strains is similar to wild type irrespective of cell length.

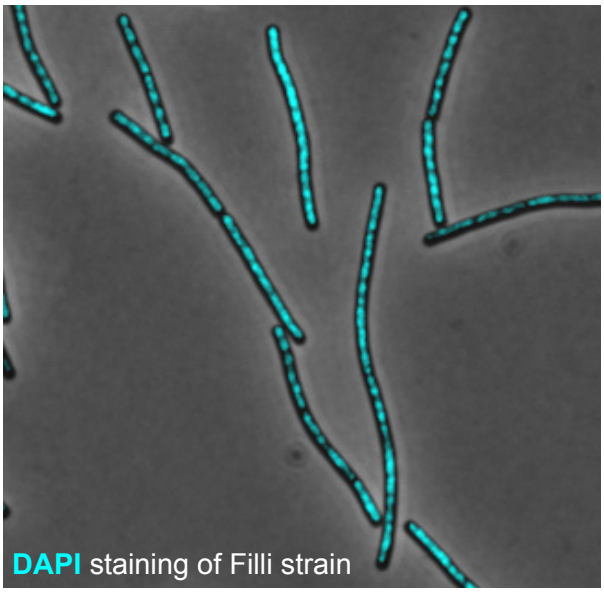

Figure S12. **DAPI staining of pre-lengthened Fili cells.** DAPI fluorescence is shown in cyan and overlaid on phase contrast images. Chromosomal DNA is regularly distributed throughout Fili cells.

S2.7. **Imaging and growth**

The general procedure for growing, preparing and imaging cells is as described [2]. Special conditions used in the current work are described where applicable.

S2.8. **Dose response and calibration of P_{hyp} activity**

To calibrate the expression of the IPTG-inducible P_{hyp} promoter used in Hyper-α_S and Hyper-α_K strains, we measured P_{hyp}-*yfp* florescence levels in cells grown on 1.5% W/V low melting agarose pads made with resuspension medium (RM) and final IPTG concentrations as indicated. The dose response curve of P_{hyp}-*yfp* as a function of IPTG is shown below (Fig. S13). Alongside P_{hyp}-*yfp* expression levels at various IPTG concentrations, we simultaneously measured the activity of the P_{comK}-*cfp* (α_K) and P_{comS}-*yfp* (β_S) promoters in wild-type non-competent cells. This allowed us to approximately calibrate P_{hyp}-*yfp* activity in units of α_K and β_S activity in non-competent cells respectively (Fig. 2).

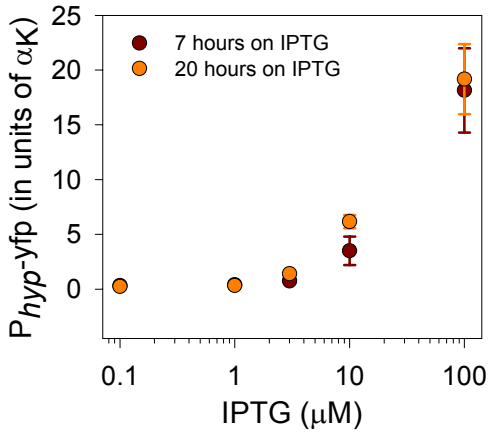

Figure S13. **Dose response of P_{hyp}-*yfp* to IPTG.** Shown are P_{hyp}-*yfp* levels as a function of log IPTG concentration. Fluorescence levels were measured at 7 and 20 hours of growth on IPTG pads as indicated alongside P_{comK}-yfp for calibration.

S2.9. Pre-lengthening protocols for the Fili strain

Fili-SOH or Fili-H strains were either induced to filament at the start of movie acquisition, or pre-lengthened prior to movie acquisition using the following protocol: After reaching an Optical Density of 1.5 in LB media with 1mM IPTG or 0.5% w/v Xylose (for Fili-SOH or Fili-H respectively), cells were pelleted and re-suspended in LB media containing no inducers (repeated twice). Cells were than grown in the absence of inducer for 60, 90 or 120 minutes to induce filamentation. After this pre-lengthening period, cells were prepared for snap shot or movie acquisition as described previously (see above and [2]).

Table S4. Statistics of Hyper-α_S and Hyper-α_K strains.

	P_{init}		Successful Exit %		Consec. Comp. Frequ.	
Strains:	**Hyper-α_K**	**Hyper-α_S**	**Hyper-α_K**	**Hyper-α_S**	**Hyper-α_K**	**Hyper-α_S**
IPTG: 0 μM	3.6 %	2.7%	62%	62%	1.5%	2.1%
1 μM	6.7 %	3.4%	66.7 %	53.3 %	7.7 %	1.02 %
3 μM	12.9 %	3.9%	54.2 %	52.5 %	38.9 %	2.8 %
10 μM	49.4 %	5.4 %	57.6 %	28.3 %	52.4 %	4.5 %
100 μM	100 %	16.9 %	0 %	21.3 %	NA	9.9 %

S3. Image quantification

S3.1. Determination of P_{init}

The probability of competence initiation (P_{init}) in movies of wild type, Hyper-α_S and Hyper-α_K strains was determined as follows: Under conditions that allow initiation of competence, as determined by increased P_{comS}-*yfp* expression levels, we picked a time window of ~150 minutes.

P_{init} was then defined as the number of competence initiation events divided by the total number of cell division events within this time frame.

S3.2. **Determination of durations**

Duration of competence events (τ_{comp}) for wild-type, Hyper-α_S, Hyper α_K and CompRok strains was determined as follows: For a given cell, we measured the time during which P_{comG}-*cfp* expression remained above 50% of its maximum level during competence. Shown below are cumulative histograms of competence duration times, for wild type and CompRok strains as indicated.

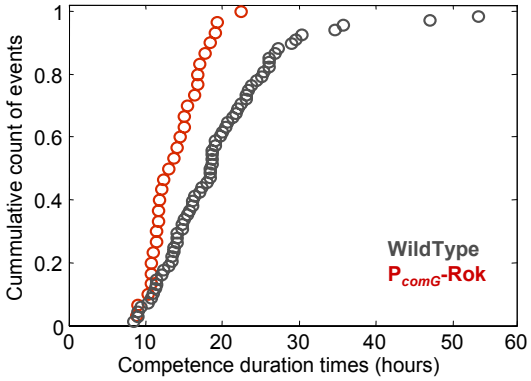

Figure S14. **Cumulative histograms of competence durations for wild type and CompRok strains.** For competence events in the CompRok strain the mean and standard deviation of the duration time of competence events is reduced (CompRok, τ_{comp} = 13.9±3.4 (n=30) hours, wild-type τ_{comp} = 20.2±9.9 (n=31) hours (mean ± s.d.).

S3.3. **Determination of cell length distributions for figure 4.**

Lengths of individual Fili-H cells were determined in phase contrast images using custom-written software (Matlab) that identifies individual cells and measures their length and P_{hyp}-*yfp* expression.

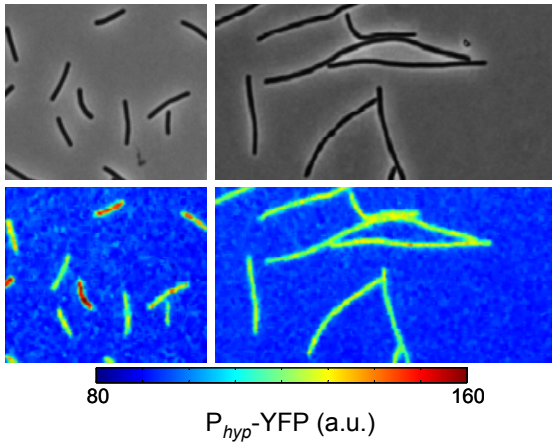

Figure S15. **Cell to cell variation in P_{hyp}-*yfp* expression in the FiliH strain.** FiliH cells at shorter lengths (left panels), exhibit more cell-cell variation in P_{hyp}-*yfp* expression compared to elongated cells (right panels) in the presence of 5µM IPTG.

In movies of Fili-SOG strains, length distribution of cells were measured using image analysis tools available with the commercially available software package ImagePro Plus. Lengths of competent cells were measured *at the point of initiation of competence* throughout the length of each movie. The lengths of non-competent cells were measured at representative time points throughout the movie. The results are shown in Fig S16.

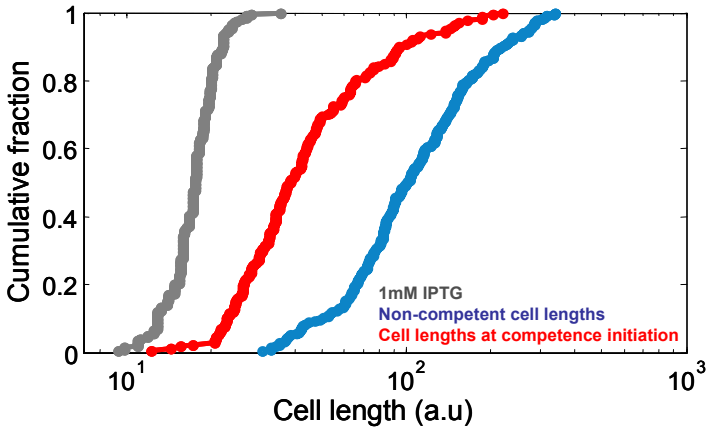

Figure S16. **Cells that initiate competence are shorter than non-competent cells.** Shown are cumulative histograms of competence initiating (red) and non-competent (blue) Fili-SOG strain cells as well as Fili-SOG strains grown in the presence of IPTG, which rescues the filamentation phenotype. The distribution of competence initiating cells is reduced compared to the overall length distribution of non-competent Fili-SOG cells.

S3.4. **Calculation of P_{init} versus length**

The calculation of P_{init} versus length determines if the length of a cell, and thus noise, affects competence initiation probability. As can be seen in the cumulative histograms in figure S16 above, the distribution of cell lengths of Fili-SOG cells grown in the absence of IPTG is, as expected, shifted to the longer cell lengths when compared to the distribution of Fili-SOG cells grown with IPTG. The distribution of cell lengths of competence initiating cells is shifted towards shorter cell lengths. To quantify this effect, distributions of both competent and non-competent cell lengths were divided into identical bins by cell length. We determined the total number of cells and the number of cells that initiated competence within each cell length bin. The fraction of competent cells within a given cell length bin is defined as P_{init}. A simple plot of P_{init} versus length shows that shorter and noisier cells (as shown in Fig.4D), are more likely to become competent than longer cells. The implications of this result are discussed in the main text.

S3.5. **PcomS and Pspo0A expression in Fili-SOG cells as a function of cell length.**

Spo0A is a master regulator of sporulation. Both, very low and high concentrations of Spo0A can inhibit competence development. Similarly, ComS is required for competence development. Therefore, we tested if the decrease in P_{init} as a function of increasing cell length (Fig. 4D) was caused by changes in expression of P_{comS} and P_{spo0A} in elongating Fili-SOG cells. As seen below, P_{comS} and P_{spo0A} expression did not change as a function of increasing cell length in Fili-SOG cells. Although these results cannot rule out all possible indirect effects on P_{init} from cell length

increase, they support the idea that expression levels of related genes are not affected by cell length.

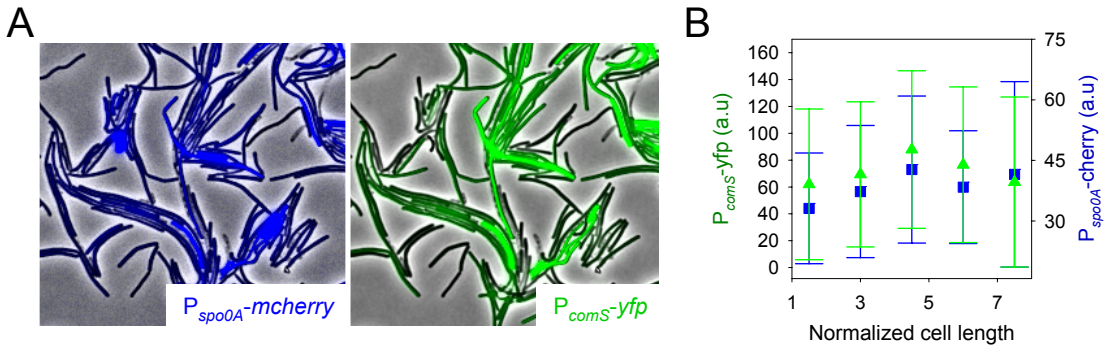

Figure S17. **P_{comS} and P_{spo0A} expression in Fili-SOG cells as a function of cell length.** (A), Expression of fluorescence from chromosomally integrated copies of P_{comS}–*mCherry* and P_{spo0A}–*yfp* (depicted in false colored blue and green respectively) was quantified as a function of cells length. (B), Expression of P_{comS} and P_{spo0A} (mean±s.d.) are not affected by cell length.

References:

1. Dubnau, D. and R. Losick, *Bistability in bacteria.* Mol Microbiol, 2006. **61**(3): p. 564-72.
2. Suel, G.M., et al., *An excitable gene regulatory circuit induces transient cellular differentiation.* Nature, 2006. **440**(7083): p. 545-50.
3. Izhikevich, E.M., *Dynamical systems in neuroscience: The geometry of excitability and bursting*. 2006: The MIT press.
4. Hodgkin, A.L., *The local electric changes associated with repetitive action in a non-medullated axon.* J Physiol, 1948. **107**(2): p. 165-81.
5. Tateno, T., A. Harsch, and H.P. Robinson, *Threshold firing frequency-current relationships of neurons in rat somatosensory cortex: type 1 and type 2 dynamics.* J Neurophysiol, 2004. **92**(4): p. 2283-94.
6. Gutkin, B.S. and G.B. Ermentrout, *Dynamics of membrane excitability determine interspike interval variability: a link between spike generation mechanisms and cortical spike train statistics.* Neural Comput, 1998. **10**(5): p. 1047-65.
7. Gillespie, D.T., *Exact stochastic simulations of coupled chemical reactions.* J. Phys. Chem., 1977. **81**: p. 2340.
8. Hoa, T.T., et al., *Rok (YkuW) regulates genetic competence in Bacillus subtilis by directly repressing comK.* Mol Microbiol, 2002. **43**(1): p. 15-26.
9. Swain, P.S., M.B. Elowitz, and E.D. Siggia, *Intrinsic and extrinsic contributions to stochasticity in gene expression.* Proc Natl Acad Sci U S A, 2002. **99**(20): p. 12795-800.
10. Resnekov, O. and R. Losick, *Negative regulation of the proteolytic activation of a developmental transcription factor in Bacillus subtilis.* Proc Natl Acad Sci U S A, 1998. **95**(6): p. 3162-7.